Proceedings of
11th European Conference on Turbomachinery Fluid dynamics & Thermodynamics
ETC11, March 23-27, 2015, Madrid, Spain

NUMERICAL ANALYSIS OF STATOR-STATOR INTERACTIONS IN A ONE AND ONE-HALF STAGE HIGH PRESSURE TURBINE

Pierre Gougeon - Ghislaine Ngo Boum

Laboratoire de Mécanique des Fluides et d'Acoustique
UMR CNRS 5509
École Centrale de Lyon - INSA Lyon - Université de Lyon
36 avenue Guy de Collongue
69134 Ecully Cedex, France

ABSTRACT

Increasing the performance of aeronautical turbines is still a matter of great interest. In particular, aerodynamic losses, generated in a first low pressure vane (LPV) when it is located downstream a highly loaded transonic high-pressure turbine (HPT), are high and still partly misunderstood. The flow complexity comes from important aerodynamic interactions between the blade rows which can mainly be classified in two types: rotor-stator interactions and stator-stator interactions. The purpose of the present study is to simulate accurately and quantify stator-stator interactions in a HPT-LPV configuration. A 3D unsteady RANS approach using both phase-lagged and multiple passages techniques is used to simulate the flow field. Specific post-treatments on the resulting unsteady flow field are used to assess the nature and the intensity of the different interactions. Numerical results are compared to experimental steady measurements in the inter-turbine duct and downstream of the LPV.

NOMENCLATURE

x-axis	Axis of rotation
θ	Circumferential direction
ω	Rotor angular velocity
Ps	Static pressure
Pta	Absolute total pressure
Tta	Absolute total temperature
α	Yaw angle
M	Mach number
S	Entropy
HPV	High-Pressure Vane
HPR	High-Pressure Rotor
HPT	High-Pressure Turbine stage (HPV followed by the HPR)
LPV	Low-Pressure Vane
GCF	Greatest Common Factor ($= GCF(N_{HPV}, N_{LPV})$)
MPPL	Multiple Passages Phase-Lagged
N_{row}	Number of blades in the row
BPF	Blade Passing Frequency $BPF = \frac{\omega N_R}{2\pi}$
$\hat{u}$	FFT amplitude
E	Total energy of the different modes

INTRODUCTION

In aeronautical turbines, the very high level of efficiency obtained when considering only the HPT is decreased when both the HPT and the first LPV are considered not only because of the single LPV losses. The intermediate turbine duct between the HPT and the LPV is the place of complex

aerodynamic phenomena. Therefore, understanding the loss mechanisms in that region and in the first LPV is an important issue in order to increase the performance of the turbine.

Aerodynamic interactions can be defined as the reciprocal effects of two blade rows on their individual flow field. In order to understand the nature of interactions, the three main aerodynamic structures present in the flow field of a transonic HPT are described here. The first ones are the result of potential field which is due to inviscid behaviour and compressibility effects. In the case of a transonic flow, shock waves appear at the blades trailing edges. Busby et. al. [3] showed that HPV and HPR trailing edge shock waves impact and reflect on the adjacent blade within the same row and also on the blades of the neighbouring row, forming then a complex grid of shock waves going forward and backward in the inter-row spacing. The potential effect spreads upstream and downstream of the row. The second structures result from viscous effects which are responsible for the formation of wakes at the blades trailing edges. Hodson and Howell [10] explained that while passing through the following blade passage, the wakes are first compressed and then chopped, bowed and stretched. Finally, the third structures, the secondary flows, have been reviewed in detail by Langston [12]: they are due to the presence of endwalls and to the deviation of a viscous boundary layer in a blade passage. Binder [2] also explained that, after developing within the blade passage, vortices are convected in the flow direction and have a strong mixing effect downstream. Contrary to shock waves, wakes and vortices only interact with downstream flow fields. These three flow structures also interact with each other generating new structures. It is the case when vortices meet wakes or more generally boundary layers. New counter-rotating vortical structures are created.

Previous experimental studies investigated a one and a half stage HPT configuration, with different inter-turbine ducts as for instance Schennach et. al [16] who studied clocking effects. Varying the pitchwise relative position of the second stator (LPV) compared to the first stator (HPV) can improve significantly the performance of the machine (1.5% efficiency increase in their case). Van Zante et. al [17] explained that the higher the Greatest Common Factor (GCF) between HPV and LPV blade number, the higher the performance of the configuration could be modified with a change of the HPV-LPV relative position.

The vane-vane interaction was detected through different investigations. Miller et. al [13] measured the pressure field on a HPR blade and revealed the presence of HPV-LPV frequencies. Hodson and Howell [10] showed that the wake avenues of stator 1 behave like non uniform spatial structures in azimuthal direction when they reach stator 2. By assessing clocking effects in a 1.5 HPT, Hummel [11] showed that HPR shock waves impact on the LPV is reduced for a specific axial position of the LPV corresponding to the HPV wakes-HPR shocks interaction.

Praisner et al. [15] underlined the importance of accounting for the HPT when computing a LP turbine because it modifies the level of unsteadiness. A previous study from the author on the same geometry (Gougeon et. al. [8]) compared the results obtained when computing the HPT configuration or the inter-turbine (HPR-LPV) configuration. The study showed that the interactions are a complex mapping of the different blade rows influence and therefore showed the importance of taking into account all the blade rows in order to reproduce all existing aerodynamic interactions. The different contributions to velocity fluctuation in the inter-turbine region was quantified: 6 to 8% (of the mean flow) come from the HPR structures, 2 to 4% from interaction modes, only 2% from the LPV when over 6% come from the HPV upstream of the rotor.

The three objectives of the present study are first to define a new strategy for the computation of the full configuration (HPT+LPV) with reasonable CPU ressources, second to analyze the flow field in comparison with previous numerical results and experimental data and finally, to evaluate the vane-vane interaction and its impact on the LPV aerodynamic losses. For confidentiality reasons, the figures featuring the turbine geometry are not drawn to scale and the periodicities are modified.

PRESENTATION OF THE STUDY

Experimental setup: facility and instrumentation

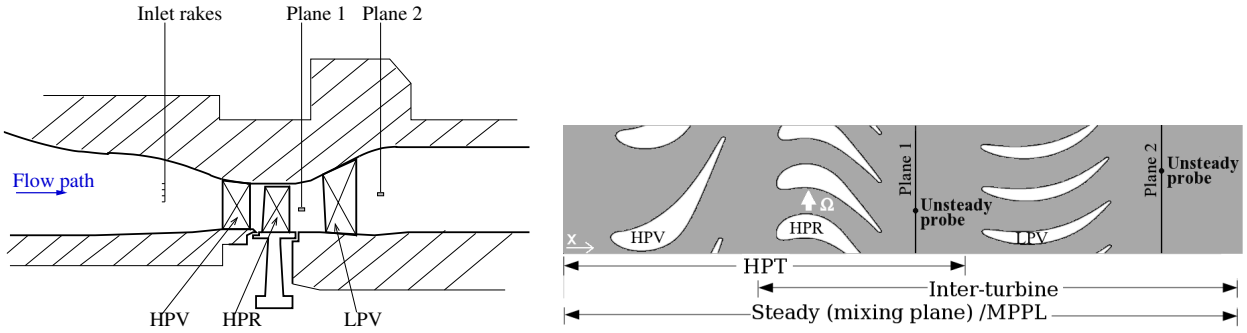

(a) Cross-sectional schematic (b) Blade to blade overview

Figure 1: **Description of the experimental one and a half stage HPT facility**

The test section is a closed loop test rig in which a reduced-scale, highly loaded, one and a half stage HPT is set. In this paper, the computation is done at the nominal operating point. Figure 1 is a schematic representation of the configuration with the approximated locations of the measurement planes. The experiments are done at transonic conditions. The blades are uncooled and the walls are assumed adiabatic. A focus is done on the inter-turbine duct and on the LPV, where two planes of measurements were defined (referred as 1 and 2, Figure 1(a) and 1(b)). Two types of measurements were done using steady (Tta, Pta and α) and unsteady probes (Pta).

Computational method

Handling a 1.5 turbine stage configuration

Time-dependent methods take into account the relative motion between the blade rows and consequently need to handle the problem of non-consistent blade count. A full annular unsteady resolution of the present configuration would be too expensive, therefore an alternative can be found using the periodicity between the blade rows and solving on the same azimuthal extent using at the rows interface, a sliding mesh method. This implies for data exchange at rows interface and at each timestep, an interpolation of the flow field on the adjacent grid with respect to its relative position. In our case, half the circumference should be computed to use a sliding mesh technique which is still a huge domain to consider.

Another alternative to handle the non-consistent blade count, is to use phase-lag approach introduced by Erdos [7]. The simulations are then efficient and reduce the computational domain to a single blade passage per row when considering two adjacent blade rows. On periodic boundaries and at rows interface, He [9] proposed to store Fourier coefficients for each conservative and turbulent variables. The harmonics corresponding to the opposite row are the only frequencies kept on the periodic boundaries. In the case where the three blade rows do not have the same number of blades, one has to define carefully the computational domain. Multiple frequency phase lagged method could be a solution if a stator-stator interaction could be represented. It is not the case with Castillon [5] approach in which a relative motion between the rows is necessary to consider the reciprocal influence.

Therefore, to simulate the flow in the present one and a half stage configuration, a simple phase-lagged approach with multiple passages accounted for stators is used. A single rotor passage is computed with phase-lagged boundary condition at stage and periodic boundaries. The same periodic pitch has then to be computed for the up and downstream stator rows. The Greatest Common Factor of the HPV and the LPV enables to define a "super-stator" with a common pitch much smaller than half the circumference. Using the same pitch also insures that all the phenomena coming from the HPV can be seen by the LPV: (N_{HPV}/GCF) HPV passages match excatly to (N_{LPV}/GCF) LPV

passages. The stator-stator interaction is entirely accounted in this Multiple Passages Phase-Lagged (MPPL) configuration. Figure 2 is a schematic drawing of the MPPL configuration. Two characteristic times appear: the rotor period $T_R = \frac{2\pi}{\Omega GCF}$ linked to the passing of the "super-stator" and the stator period $T_S = \frac{2\pi}{\Omega N_{HPR}}$ linked to the passing of rotor blades.

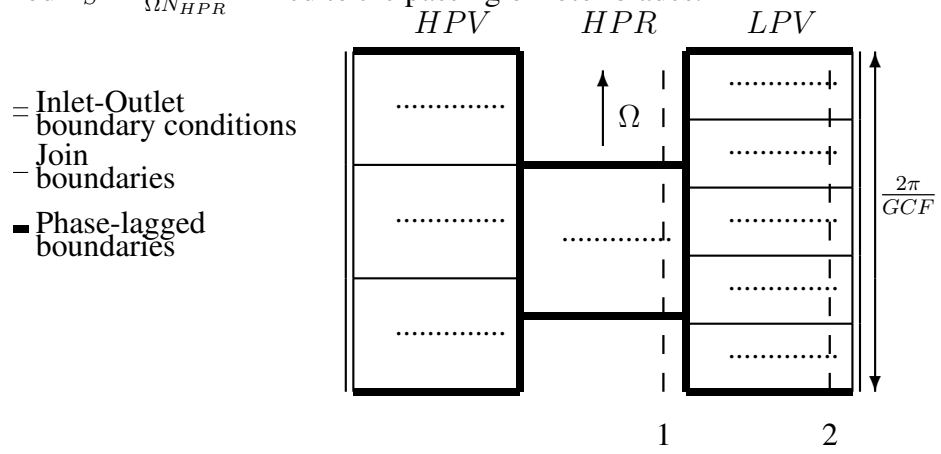

Figure 2: **Computational domain of the MPPL simulation: theorethical scheme (the true periodicities are not shown).**

Numerical settings

Details of the numerical simulation were assessed in the previous article (Gougeon et. al.[8]) and the results with the simple phase-lagged computations on the HPT and the inter-turbine computation are compared to the MPPL solution, as well as steady mixing plane results. The different configurations and the axial extent of the computational domains are presented on figure 1(b). Simulations are carried out with the compressible flow solver *elsA* developed by ONERA (French Aerospace lab, Cambier [4]). The meshes have been validated for two different (coarse and fine) distributions. y^+ is less than 1 for the major part of the walls and less than 5 in the whole configuration. For unsteady simulations, the mesh enables to take into account at least 30BPF (rotor Blade Passing Frequency). The phase-lag and blade passing periods are full multiple of the timestep. Backward-Euler scheme is used for the time integration and for space discretization, Roe scheme with a third order limiter is used. Turbulence is solved with the *Explicit Algebraic Reynolds Stress Model* (EARSM) which is an advanced turbulence model. The model showed best results for losses prediction in the LPV in the previous study (Gougeon et. al.[8]). The inlet boundary conditions are deduced from the measurements done with probe rakes (stagnation pressure and temperature, velocity direction). Adiabatic conditions are set on the walls. The outlet boundary condition is a linear static pressure distribution extrapolated from the pressure measured in plane 2 (downstream LPV figure 1 (b)).

Mass flow convergence in the MPPL method

After a time period corresponding to 1.5 revolution of the rotor, computation convergence is observed on inlet-outlet mass flow balance and static pressure and temperature monitoring at different locations in the domain. The mass flow rate is plotted on figure 3(left) for the last passing periods. The signal periodicity testifies that a periodic state is indeed reached. The relative mass flow rate difference between two equivalent instants of the last computed period N and the preceding period (N-1)is computed. It is lower than 0.25% in all rows as shown on figure 3 right.

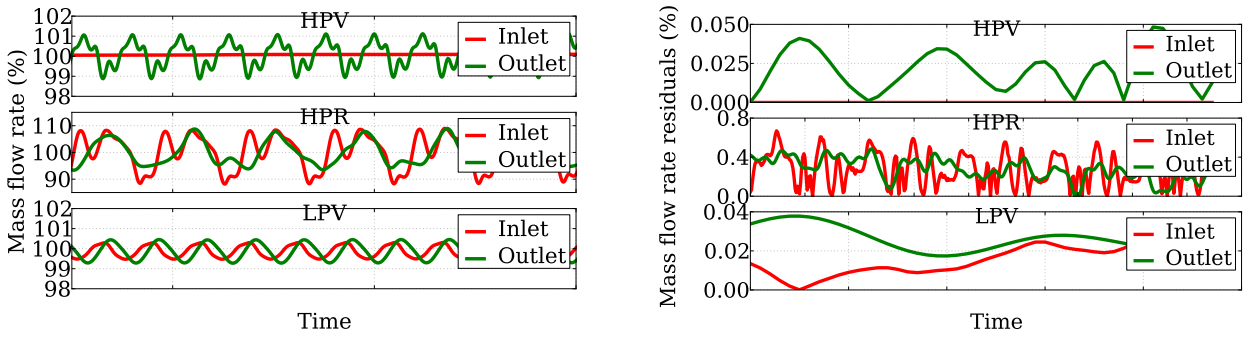

Figure 3: **Mass flow rate instantaneous signal, Q(t) (left) and residuals (Q(t)-Q(t-$T_{R,S}$)) (right)**

AERODYNAMIC FIELD

Blade to blade overview

The instantaneous aerodynamic field is shown on figure 4 at mid-span. The entropy field (left figure) reveals the convection of the wakes. As previously observed by Hodson [10] and Miller [13], HPV wake avenues are present, uptream of the LPV. The red arrows illustrate the path of one avenue through and downstream the HPR . A change of direction in the HPR is visible. Regions of high (wake) and low entropy alternate through the LPV. Contours of static pressure (right figure) show pressure waves, that is to say the shocks coming from the HPV and the HPR trailing edges and their reflections on the walls (green arrows). In the HPV-HPR channel, the interaction is stronger than in the HPR-LPV channel because of the tighter inter-row spacing. Results of an FFT done on the static pressure signals registered at different locations in and downstream of the HPR passage (yellow dots on figure 4) are plotted on figure 5. The signals are registered in the HPR rotating frame, HPV and LPV influences appear then as unsteady fluctuations. HPV harmonics are marked with green numbers and LPV harmonics with red ones. Only the HPV potential field is present upstream the HPR when downstream, only the LPV potential field is present.

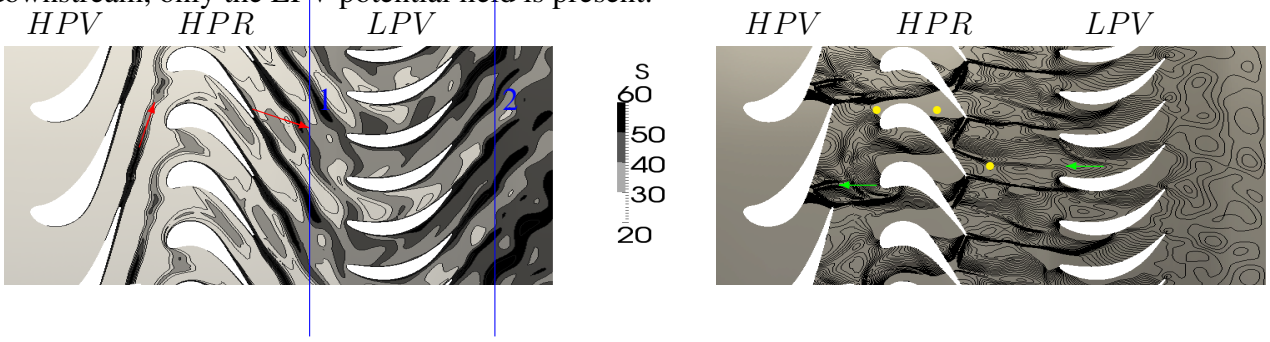

Figure 4: **Blade to blade overview at mid span for entropy (left) and static pressure (right)**

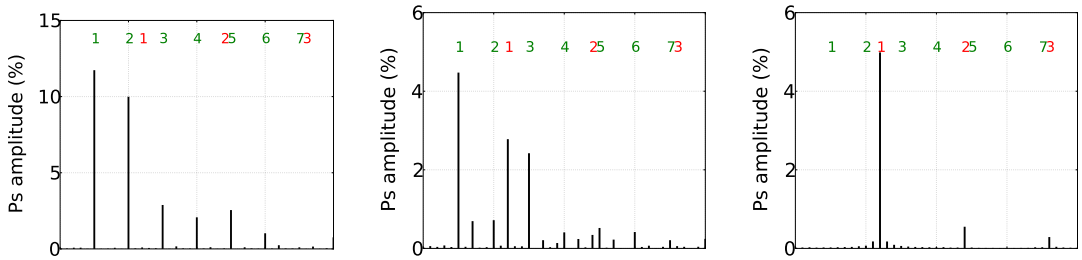

(a) Upstream HPR **(b) Within HPR** **(c) Downstream HPR**

Figure 5: **Static pressure probes (percentage of the time-averaged static pressure).**

However, the behaviour whithin the HPR passage is more complex and shows that both vanes are interacting with the HPR. The LPV influence is due to the reflexion of a HPR shock wave on its leading edge, and the HPV influence is directly linked to its trailing edge shock waves that are impacting the HPR passage field. It is remarkable that this last influence (which can reach more than 10% of Ps) disappear completely at the HPR exit. Finally, LPV harmonics are weaker and interaction frequencies (which are nonzero amplitudes between two harmonic frequencies, between 1 and 2 for example) can be identified: the vane-vane interaction is already present in the HPR channel, but its magnitude is 5 times weaker than the main HPV or LPV amplitudes. As a conclusion, FFT of the signal shows that, contrary to the wakes, the influence of the potential flow does not seem to be transmitted downstream of the HPR, which is consistent with the Ps measurements made by Miller et. al. [13] on a HPR blade.

Comparison of numerical results against experimental data in planes 1 and 2

Radial evolutions

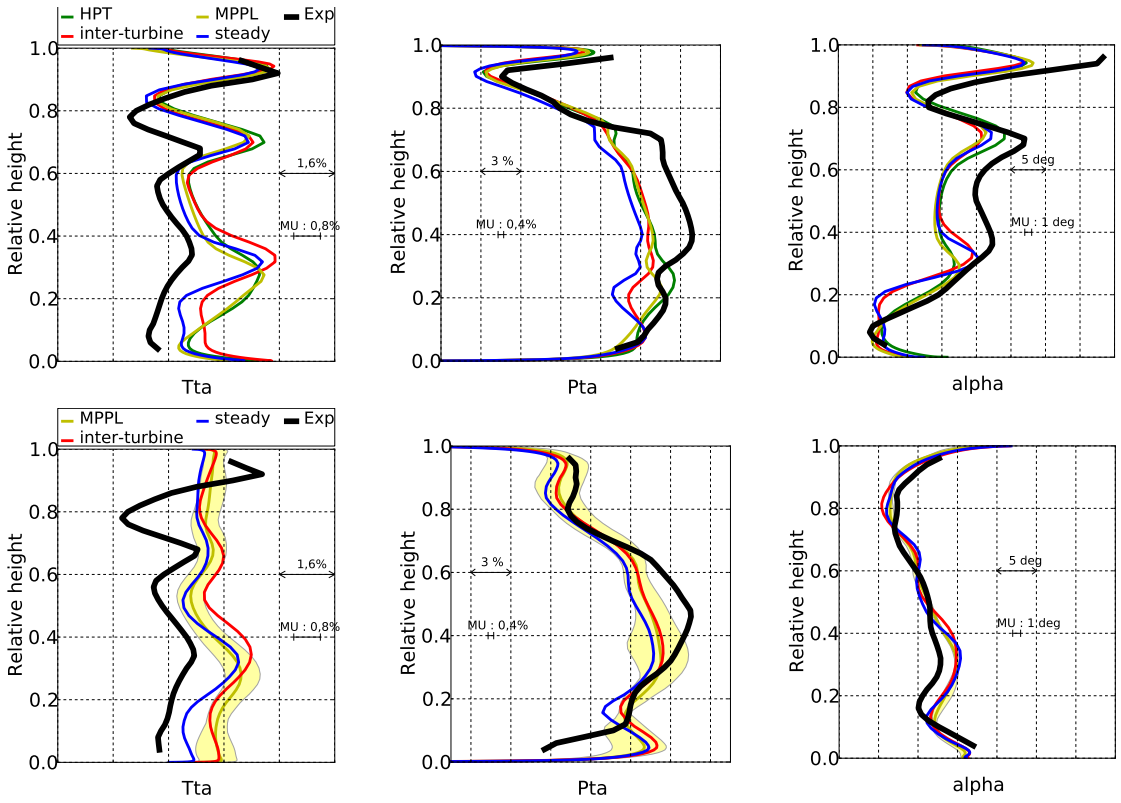

Figure 6: **Radial evolutions in sections 1 (top) and 2 (bottom). MU=Measurement Uncertainty**

In planes 1 and 2 (figure 6), a time and space average of the flowfield is done for total pressure, total temperature and angle α. The results of the computations (steady mixing plane, single HPT, inter-turbine and current MPPL (see figure 1 (b))) are compared to the experiments.

In plane 1, the radial variations are due to the presence of the different vortices: (hub and shroud passage vortices and tip gap vortex). These gradients are quite well reproduced by the simulations. No significant difference between the MPPL result and the previous results can be observed. The temperature is still overestimated meaning that the work done in the HPT is underestimated. The angle is also underestimated, except close to the hub. Plane 1 is located at the rotor exit upstream the LPV, therefore the vane-vane influence on the mean flow is negligible which explains the weak differences observed.

In plane 2, a time and space average is done for all the LPV passages computed. To visualise the

range of variation of the different quantities depending on the relative position of the LPV compared to the HPV, each passage is considered separately. A yellow strip is plotted representing the range between the minimum and maximum value obtained at each height, from hub to casing. It illustrates the spatial fluctuation corresponding to vane-vane influence. The MPPL computation does not change the time average level already obtained from the steady and unsteady previous simulations but it gives an interesting information on the vane-vane interaction which is around 0.8% of the time and space average for Tta, and varies from 1 to 4% for Pta depending on the radial position. This influence is very weak on α.

The difference between numerical simulation and experiments are higher than measurements uncertainties range for Pta and α. On the contrary, Tta measurement uncertainties are close to 1% of the average. Numerical results are then quite accurate with respect to the experiments.

Unsteady total pressure FFT in plane 1

Total pressure FFT were done in the experiments at mid-span and for two azimuthal positions. For the computations, the FFT post-processing is performed at the same axial position and for different positions at mid-span. Time FFT of the numerical results can only show the Blade Passing Frequency

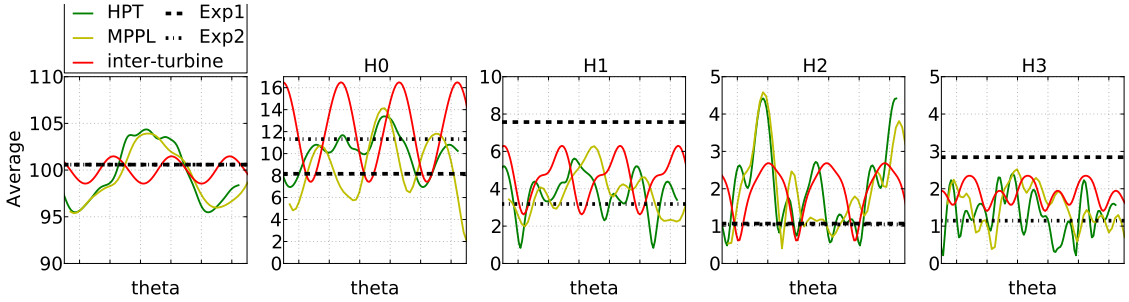

Figure 7: **Azimuthal evolution of total pressure FFT first harmonics at mid-span in plane 1 (percentage of the space and time averaged value in plane 1)**

(BPF) and its harmonics (because of the phase-lagged approach used). Therefore, on figure 7 are plotted the time-averaged signal for a line at mid-span and the first four harmonics (0 to 3) and this for the different simulations done. The two horizontal dotted lines mark the level of the two measurements on each FFT component.

In terms of mean level, the time averaged and first harmonic are well predicted by the simulations. For harmonics 1 and 3, the amplitude is underestimated by every simulation, which seems to be counter-balanced with H2 which is always greater in the computations than in the experiments. The azimuthal trends are linked to the HPV and LPV spatial positions. Time-averaged, harmonics 1 and 2 MPPL amplitudes are remarkably close to the HPT results. On the other hand harmonics 0, 1 and 3 are closer to the inter-turbine simulation result. The different aerodynamic phenomena in the MPPL case are strongly coupled all rows being computed together.

ADAMCZYK ANALYSIS

Averaged results in the configuration

The Adamczyk analysis [1] consists in a decomposition of the flow using time and space averages. The field of a quantity u can be divided into four parts:

$$u(x,r,\theta,t) = u_0(x,r) + u''_S(x,r,t) + u''_R(x,r,\theta-\omega t) + u^*(x,r,\theta,t) \quad (1)$$

with $u_0(x,r)$ the axisymmetric field resulting from a time and circumferential average, $u''_S(x,r,t)$ the spatial fluctuations in the stator frame, $u''_R(x,r,\theta-\omega t)$ the spatial fluctuations in the rotor frame

and $u^*(x, r, \theta, t)$ the unsteady interaction fluctuations. The quadratic average of each fluctuation is computed in axial sections within the inter-turbine channel and downstream the LPV on figure 8 for Ps and V. Parker exponential law [14] on potential field is also plotted for Ps.

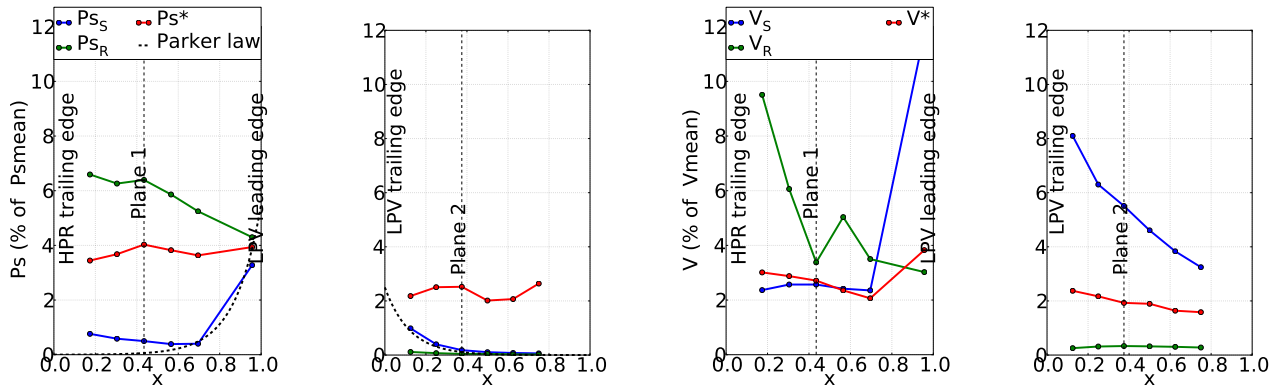

(a) Ps **upstream LPV** (b)Ps **downstream LPV** **(c)** V **upstream LPV** **(d)** V **downstream LPV**

Figure 8: **Axial evolution of Adamczyk contributions upstream and downstream LPV.**

A good agreement is shown with the LPV static pressure fluctuation (upstream and downstream) with an exponentially decreasing influence with the distance to the vane. Plane 1 is outside the potential influence zone of LPV and spatial fluctuations on Ps from HPV (shock waves for instance) are dissipated at that location. For velocity decomposition, the stator component is also higher close to the vane and it is the dominant fluctuation downstream of the LPV where its wakes are responsible for a deficit of V. For both quantities, the rotor fluctuation is dominant (around 5%) in the inter-turbine duct while it becomes negligible downstream of the LPV. The unsteady contribution is around 2% of the mean flow downstream: it is the dominant effect for Ps and second for V which can be caused by any HPV-HPR or HPV-LPV-HPR interaction. In comparison with the results obtained in a HPT computation and an inter-turbine computation (Gougeon[8]), this new configuration appears to combine both results as it shows mainly the HPT configuration behaviour in the first part of the inter-turbine duct and then the inter-turbine configuration behaviour close to the LPV and downstream of the LPV.

The Adamczyk decomposition gives a first estimation of the interaction level which is consistent in plane 2 with the estimation of stator-stator influence of 4% of the time and space average of Pta obtained in the previous section.

Spatial modes in plane 1

To understand the origins of the different spatial contributions, Adamczyk spatial fluctuations are represented for the different cases in plane 1. On figure 9, stator fluctuations of Pta are plotted on two HPV pitches. The pattern observed in the experimental results, (9 a), correspond to HPV wakes. MPPL and HPT simulations are very close to the experiments with similar fluctuations level around 5%. HPV effect is well predicted. Inter-turbine simulation shows the LPV potential field with a different periodicity and lower fluctuations amplitude, ($\pm 1\%$).

From the Adamczyk stator contribution computed in the plane, a spatial FFT is done in the azimuthal direction: $u_S(r, \theta) \quad - FFT_\theta \rightarrow \quad \hat{u}_S(r, m_\theta)$. Because the blade number count of the two stators are different, the spatial modes m_θ are separated and the effect of each blade row can then be identified. The modes are linked to the HPV, LPV or the 'super-stator' HPV-LPV. The energy associated with all the spatial modes linked to each vane (3-4-5) can be computed and expressed as a L2 norm (Courtiade et. al. [6]):

$$E_{vane}(r) = \sqrt{\sum_{N_{vane} \in m_\theta} \hat{u}_S^2(r, m_\theta)} \quad vane = HPV, LPV or HPV - LPV \tag{2}$$

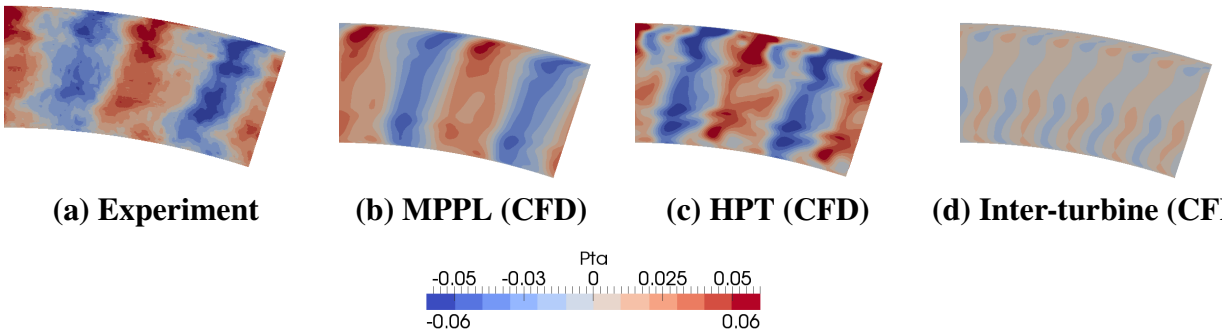

(a) Experiment **(b) MPPL (CFD)** **(c) HPT (CFD)** **(d) Inter-turbine (CFD)**

Figure 9: **Total pressure spatial fluctuations in plane 1. (Pta plotted =** $Pta"_S$ **/ (average of Pta))**

On figure 10, the decomposition of the spatial contribution is plotted in plane 1. The level of Ps fluctuations is weak (0.1 to 0.5 %) compared to Pta (0.5 to 4%) and Tta (0.1 to 1.2%): the potential effects are not dominant in this plane for each of the stators (equivalent Ps mean level around 0.4%). For Tta and Pta, the influence of HPV is clearly dominant whatever the radial position (about 4 times higher than the LPV influence). The important radial modulations, mostly on Tta curve, are due to the presence of HPV vortices. For each quantity, the vane-vane mode is very weak (less than 0.5%), which seems logical since LPV upstream effects are also very small (less than 1%).

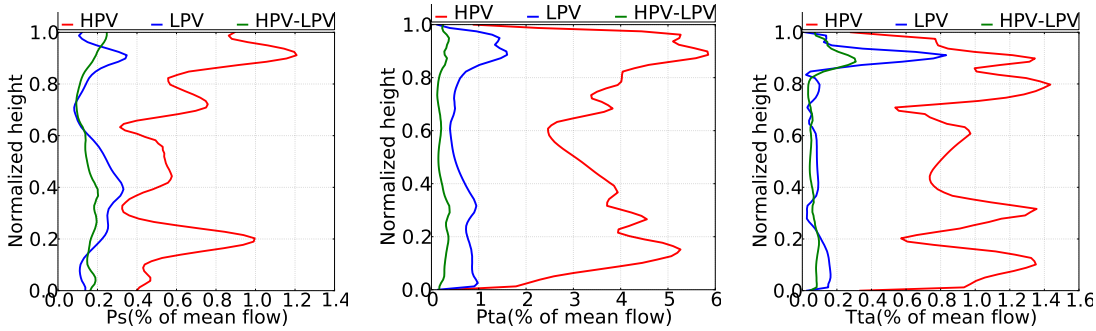

(a) Static pressure (b) Total pressure (c) Total temperature

Figure 10: **Radial evolution of the amplitudes of the spectrum of spatial modes in plane 1.**

Spatial modes in plane 2

The same analysis is done in plane 2, downstream of the LPV. On figure 11, Adamczyk spatial fluctuations of total pressure are plotted on two and a half LPV pitches. The main periodicity observed in all the plots is due to the LPV wakes. The field is totally periodic for steady and inter-turbine computations, while for the experiment and MPPL case, a new contribution which breaks that periodicity is perceived through the wakes intensity which varies (low level region of Pta are not identical). The wakes curvature and the low deficit of total pressure in the experiments are not well reproduced by the simulations.

On figure 12, the influence of the different spatial modes are plotted in plane 2. Fluctuations of Ps are again very weak compared to the other quantities, less than 0.2% of the mean Ps. For static and total pressure, LPV modes are dominant. HPV and HPV-LPV modes are equivalent and lower. This can also be observed on Pta, where the influence of the LPV wakes can be added, and the contribution rises to 4% of the mean flow. HPV contribution can reach more than 2% of the total pressure average in the plane which justifies the modulation of the periodicity in total pressure on figure 11. The behaviour of Tta is different: LPV and HPV-LPV are equivalent (around 0.2%) and much lower than that of the HPV which is clearly dominant (from 0.4 to 0.95%) along the whole span.

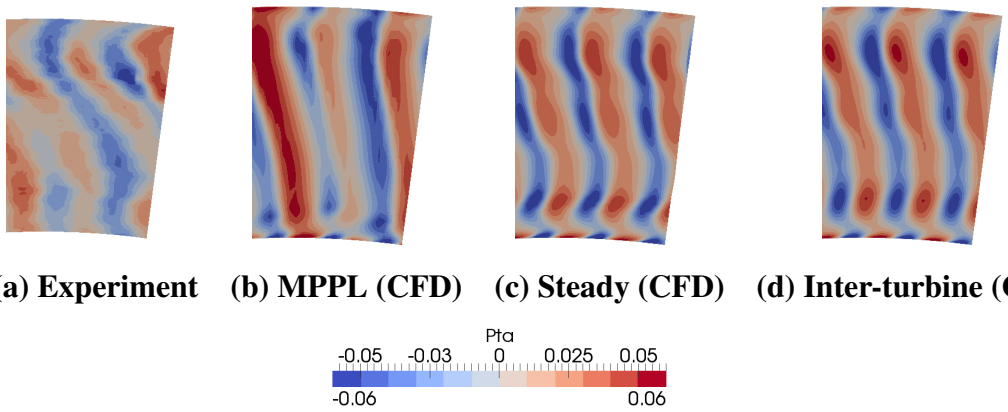

(a) Experiment **(b) MPPL (CFD)** **(c) Steady (CFD)** **(d) Inter-turbine (CFD)**

Figure 11: **Total pressure spatial fluctuations in plane 2. (Pta is plotted as a ratio of $Pta"_S$ on the average of Pta in plane 2)**

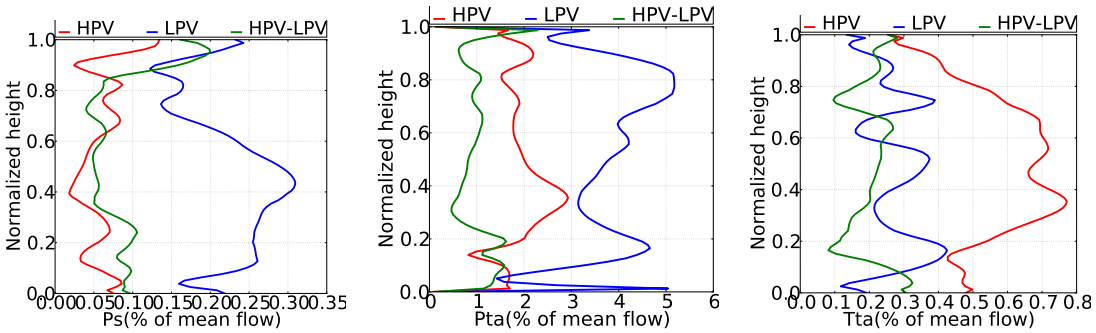

(a) Static pressure (b) Total pressure (c) Total temperature

Figure 12: **Radial evolution of the amplitudes of the spectrum of spatial modes in plane 2.**

The analysis of the spatial modes showed that the HPV mode is always dominant in the whole one and a half stage HPT. The LPV influence is perceived mainly downstream of the vane. The spatial interaction modes (HPV-LPV) are minor but their magnitude increases after the LPV, especially for total pressure and temperature. HPV wakes convected through the configuration are responsible of these effects.

LOSSES IN THE LPV

The normalized total pressure losses DP/P are defined as the ratio of the numerical total pressure losses $(1 - Pt/Pt_1)$ to the experimental total pressure losses between planes 1 and 2 $(1 - Pt_2/Pt_1)$. The measurement were done in a window corresponding to two and a half LPV pitches in plane 2. MPPL computation takes into account more LPV pitches, so different post-processing are done for comparison. First, the losses are evaluated taking into account all the computed LPV passages. The result plotted with the black line on figure 13 is very close to the inter-turbine result and also to the steady result (except for the step at mixing plane). Then to estimate the losses variation depending on the azimuthal position, a pitchsize equivalent to the experimental pitchsize is considered to evaluate losses. Reference is taken at LPV leading edge to consider the same mass flow along the axial direction for each losses evaluation. The min-max values are plotted with the yellow strip on figure 13, left. The fluctuations around the average value are about $\pm 4\%$ and represent the vane-vane interaction. On figure 13 right, losses are computed for each single passage of the LPV vane. From a passage to another, DP/P varies significantly and the min-max envelop plotted represents 35% at the trailing edge. The strong HPV influence which generates important spatial fluctuations at LPV inlet is responsible for that variation. Vane-vane interaction has therefore a non negligeable contribution to

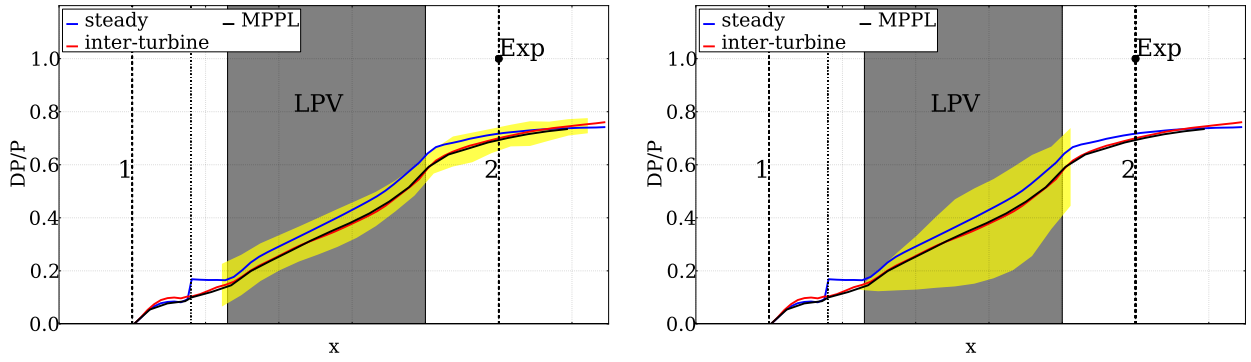

Figure 13: **LPV total pressure losses (yellow min-max envelop with 3 (left) or 1 (right) LPV passages considered)**

pressure losses.

CONCLUSION

In this study, a time-accurate numerical approach which takes into account the unsteady effects through a phase-lagged technique and stator-stator interactions through a multiple passages approach, has been assessed. This MPPL approach was able to compute the interaction between the different blade rows.The analysis performed using Adamczyk decomposition and then a modal decomposition allowed to identify precisely the influence of each blade row at two locations in the configuration.

In plane 1 between HPR and LPV, the HPV influence is dominant due to its wake and vortices. The LPV potential effect is 4 times weaker than HPV fluctuation on Pta and decreases exponentially when moving axially upstream of the LPV. The fluctuations associated to HPV-LPV interaction are negligible at that location.

In plane 2 downstream the LPV, HPV influence is persistent. Therefore, computing the whole configuration is necessary to capture stator-stator interaction but it is not sufficient to fill the gap between numerical loss predictions in the LPV passage and experimental measurements. However, the important azimuthal fluctuations existing makes it difficult to compute rigorously total pressure losses when the pitchsize considered during the experiments does not guaranty a consistent massflow between plane 1 and plane 2. Part of the difference observed between numerical and experimental results may take their origin there as losses appear to be steady.

Investigating on turbulence modelling to restitute the complex turbulent structures identified in the configuration may also be an issue to further understand differences between the prediction and the experiments. In the same idea, the mean value of the Reynolds number at LPV inlet is about $1.7e+6$, then an intermittent laminar-turbulent transition on LPV could be present and generate significant extra losses if a separation exists.

ACKNOWLEDGEMENTS

The authors are thankful to late Pr. Francis Lebœuf who had provided helpful guidelines on this study. They are also grateful to Snecma (Safran Group) for providing access to experimental results obtained with the participation of Von Karman Institute and authorizing the publication of the work they support. This computation was performed using HPC resources from the Fédération Lyonnaise de Calcul Hautes Performances (FLCHP) and from GENCI-[CCRT/TGCC/CINES/IDRIS](Grant 2012 - i2012021594, Grant 2013 - c20132a1594) and from FLMSN-[PMCS2I].

References

[1] J. J. Adamczyk. Model Equation for Simulating Flows in Multistage Turbomachinery. *ASME Paper 85-GT-226*, 1985.

[2] A Binder. Turbulence Production Due to Secondary Vortex Cutting in a Turbine Rotor. *Journal of Engineering for Gas Turbines and Power*, 107(October 1985):1039–1046, 1985.

[3] J A Busby, R L Davis, D J Dorney, M G Dunn, C W Haldeman, R S Abhari, B L Venable, and R A Delaney. Influence of Vane-Blade Spacing on Transonic Turbine Stage Aeodynamics: Part II – Time-Resolved Data and Analysis. *Journal of Turbomachinery*, 121(October 1999):673–682, 1999.

[4] L Cambier, M Gazaix, S Heib, S Plot, M Poinot, and M Montagnac. An Overview of the Multi-Purpose elsA Flow Solver. *CFD Platforms and Coupling*, (2):1–15, 2011.

[5] L Castillon. Evaluation of a multiple frequency phase lagged method for unsteady numerical simulations of multistage turbomachinery. In *28th International Congress of the Aeronautical sciences*, 2012.

[6] N. Courtiade, X. Ottavy, and N. Gourdain. Modal decomposition for the analysis of the rotor-stator interactions in multistage compressors. *Journal of Thermal Science*, 21(3):276–285, May 2012.

[7] J. I. Erdos, E. Alzner, and W. McNally. Numerical Solution of Periodic Transonic Flow through a Fan Stage. *AIAA Journal*, 15(11):1559–1568, 1977.

[8] P. Gougeon and G. Ngo Boum. Aerodynamic Interactions Between A High Pressure Turbine And The First Low Pressure Stator. *Journal of Turbomachinery*, 136(7), 2014.

[9] L He. An Euler Solution for Unsteady Flows Around Oscillating Blades. *Journal of Turbomachinery*, 112:714–722, 1990.

[10] H P Hodson and R J Howell. Unsteady Flow: Its Role In the Low Pressure Turbine. In *9th International Symposium on Unsteady Aerodynamics, Aeroacoustics and Aeroelasticity of Turbomachines, Lyon*, 2000.

[11] Frank Hummel. Wake-Wake Interaction and Its Potential for Clocking in a Transonic High-Pressure Turbine. *Journal of Turbomachinery*, 124(1):69, 2002.

[12] L. S. Langston. Secondary Flows in Axial Turbines - A review. *Annals of the New York Academy of Science*, pages 11–26, 2001.

[13] R. J. Miller, R. W. Moss, R. W. Ainsworth, and N. W. Harvey. Wake, Shock, and Potential Field Interactions in a 1.5 Stage Turbine-Part II: Vane-Vane Interaction and Discussion of Results. *Journal of Turbomachinery*, 125(1):40, 2003.

[14] R. Parker and J. F. Watson. Interaction Effects between Blade Rows in Turbomachines. In *Proceedings of the Institution of Mechanical Engineers*, volume 186, pages 331–340, 1972.

[15] T. J. Praisner, E. Grover, R. Mocanu, R. Jurek, and R. Gacek. Predictions of Unsteady Interactions Between Closely Coupled HP and LP Turbines With Co- and Counter-Rotation. *Volume 7: Turbomachinery, Parts A, B, and C*, pages 2715–2724, 2010.

[16] O. Schennach, J. Woisetschläger, B. Paradiso, G. Persico, and P. Gaetani. Three Dimensional Clocking Effects in a One and a Half Stage Transonic Turbine. *Journal of Turbomachinery*, 132, 2010.

[17] Dale Van Zante, Jenping Chen, Michael Hathaway, and Randall Chriss. The Influence of Compressor Blade Row Interaction Modeling on Performance Estimates From Time-Accurate, Multistage, Navier-Stokes Simulations. *Journal of Turbomachinery*, 130(1):011009, 2008.